Article

Cell Reports

Alterations in Phosphorylation of Hepatocyte Ribosomal Protein S6 Control *Plasmodium* Liver Stage Infection

Graphical Abstract

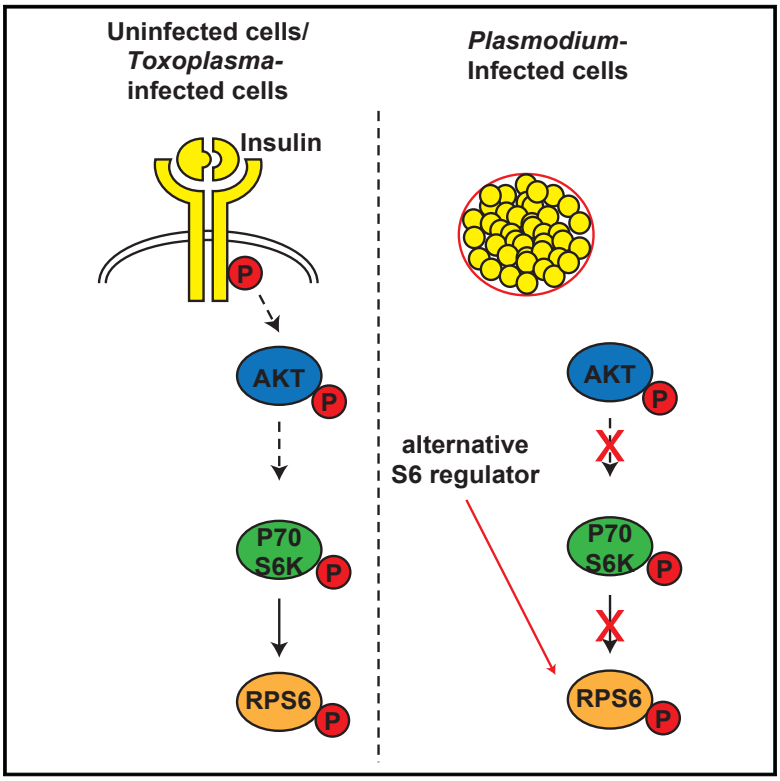

Highlights

- p-RPS6 is elevated in hepatocyte populations susceptible to *Plasmodium* (*Py*)
- Inhibiting RPS6 phosphorylation prior to infection decreases *Py* infection
- In *Py*-infected hepatocytes, canonical Akt/ RPS6 signaling is disrupted
- Response to insulin is abrogated in *Py*-infected hepatocytes

Authors

Elizabeth K.K. Glennon, Laura S. Austin, Nadia Arang, ..., John D. Aitchison, Stefan H.I. Kappe, Alexis Kaushansky

Correspondence

alexis.kaushansky@seattlechildrens.org

In Brief

After mosquito-to-human transmission, *Plasmodium* parasites infect hepatocytes. Glennon et al. demonstrate that infected cells exhibit elevated levels of ribosomal protein S6 phosphorylation, and this phosphorylation appears uncoupled from canonical regulators. This work raises the possibility that *Plasmodium*-infected hepatocytes are governed by non-canonical, re-wired signal transduction cascades.

Glennon et al., 2019, Cell Reports *26*, 3391–3399
March 19, 2019
https://doi.org/10.1016/j.celrep.2019.02.085

CellPress

Cell Reports
Article

Alterations in Phosphorylation of Hepatocyte Ribosomal Protein S6 Control *Plasmodium* Liver Stage Infection

Elizabeth K.K. Glennon,[1,2,3] Laura S. Austin,[1,5] Nadia Arang,[1,6] Heather S. Kain,[1] Fred D. Mast,[1,2,4] Kamalakannan Vijayan,[1,2] John D. Aitchison,[1,2,4] Stefan H.I. Kappe,[1,2,3] and Alexis Kaushansky[1,2,3,7,*]
[1]Center for Infectious Disease Research, Seattle, WA 98109, USA
[2]Seattle Children's Research Institute, Seattle, WA 98109, USA
[3]Department of Global Health, University of Washington, Seattle, WA 98109, USA
[4]Institute for Systems Biology, Seattle, WA 98109, USA
[5]Present address: Clover Park Technical College, Lakewood, WA, USA
[6]Present address: Biomedical Sciences Graduate Program, University of California, San Diego, 9500 Gilman Drive, La Jolla, CA 92093, USA
[7]Lead Contact
*Correspondence: alexis.kaushansky@seattlechildrens.org
https://doi.org/10.1016/j.celrep.2019.02.085

SUMMARY

Plasmodium **parasites are highly selective when infecting hepatocytes and induce many changes within the host cell upon infection. While several host cell factors have been identified that are important for liver infection, our understanding of what facilitates the maintenance of infection remains incomplete. Here, we describe a role for phosphorylated ribosomal protein S6 (Ser235/236) (p-RPS6) in *Plasmodium yoelii*-infected hepatocytes. Blocking RPS6 phosphorylation prior to infection decreases the number of liver stage parasites within 24 h. Infected hepatocytes exhibit elevated levels of p-RPS6 while simultaneously abrogating the induction of phosphorylation of RPS6 in response to insulin stimulation. This is in contrast with the regulation of p-RPS6 by *Toxoplasma gondii,* which elevates levels of p-RPS6 after infection but does not alter the response to insulin. Our data support a model in which RPS6 phosphorylation is uncoupled from canonical regulators in *Plasmodium*-infected hepatocytes and is relied on by the parasite to maintain infection.**

INTRODUCTION

Plasmodium parasites are the causative agents of malaria and inflict substantial disease worldwide. Malaria disease is caused by the intraerythrocytic forms of the parasite, which multiply rapidly in the blood, causing fever, anemia, and complications in multiple organs (Trampuz et al., 2003). To establish intraerythrocytic infection, parasites first interact with the dermis (Gueirard et al., 2010), enter the circulation, travel to the liver, and then undergo obligate intracellular development within the liver. Unlike other apicomplexan parasites, particularly *Toxoplasma gondii*, when *Plasmodium* parasites are transmitted to the human host, they are exquisitely selective for their first host cell, the hepatocyte. No clinical symptoms are associated with liver stage (LS) infection, and parasite numbers are extremely low, suggesting that this point of development represents a bottleneck for the parasite (Vaughan et al., 2008). Thus, LS represents an attractive target for intervention.

During LS infection, intracellular parasites dramatically alter the biology of their hepatocyte host cells. For example, LS parasites divide tens of thousands of times, stretching the host cell to 50–100 times its normal volume, despite the presence of regulatory pathways that carefully control hepatocyte size (Sinturel et al., 2017). Hepatocytes initiate a range of host defense pathways upon *Plasmodium* infection, including apoptosis (Kaushansky et al., 2013), autophagy (Thieleke-Matos et al., 2016), and multiple classical innate immune responses such as the Type I interferon response (Liehl et al., 2014, 2015; Miller et al., 2014). Moreover, not all hepatocytes have an equivalent capacity to support sporozoite infection. Human hepatocytes from different donors show differential susceptibility *in vitro* (March et al., 2013), and mice of different strains have dramatically different susceptibilities to LS infection, even those that are genetically closely related (Khan and Vanderberg, 1991; Scheller et al., 1994). Specifically, hepatocytes from the mouse substrain BALB/cByJ exhibit a 2- to 5-fold increased susceptibility compared to those from BALB/cJ mice (Kaushansky et al., 2015a). Even within a single animal, cellular properties, such as the DNA content of hepatocytes, have been associated with infection, as polyploid hepatocytes are more susceptible to infection than diploid hepatocytes (Austin et al., 2014). Polyploidy is a common feature of hepatocytes in both mice and humans and is thought to play a role in liver regeneration (Øvrebø and Edgar, 2018).

The specific host factors supporting parasite development are not comprehensively understood; however, several hepatocyte membrane proteins, including EphA2, CD81, and SR-BI, have been identified to play a significant role in mediating parasite invasion (Kaushansky et al., 2015b; Silvie et al., 2006; Yalaoui et al., 2008). Once a parasite is inside a hepatocyte, its survival is also influenced by host cell factors, including levels of the tumor suppressor p53 (Douglass et al., 2015; Kaushansky et al., 2013),

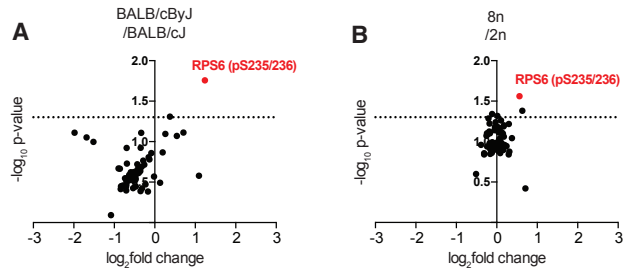

Figure 1. Phosphorylated Ribosomal Protein S6 Is Elevated in *P. yoelii*-Susceptible Cell Populations

(A and B) Log_2 fold change in RPPA signal plotted against $-log_{10}$ p value for each of 62 antibodies against total or phosphorylated protein in (A) livers of BALB/cByJ (n = 10) compared to BALB/cJ (n = 10) mice and (B) 8n, compared to 2n, hepatocytes isolated from 10 BALB/cAnN mice. Signal from each antibody was normalized to β-actin.

Table 1. Top Differentially Regulated Total and Phosphorylated Proteins in Susceptible Cell Types

Antibody	Fold Change	SE	p Value
BALB cByJ/cJ Upregulated			
RPS6 (pS235/236)	1.477	0.041	0.027
SOD2	1.548	0.065	0.042
DUSP4	1.231	0.075	0.061
Glycogen synthase (pS641)	1.296	0.117	0.091
8n/2n Upregulated			
RPS6 (pS236/236)	2.359	0.074	0.017
EGFR	1.297	0.064	0.049
Dvl3	1.634	0.067	0.077
Heregulin	1.200	0.016	0.080
SOD2	1.460	0.086	0.085
BALB cByJ/cJ Downregulated			
Jak2	0.765	0.084	0.109
8n/2n Downregulated			
EIF4E	0.253	0.072	0.078
FAK (pY397)	0.793	0.062	0.078
ERK (pT202/Y204)	0.311	0.142	0.089
PTEN	0.349	0.127	0.100

Twenty percent fold change and a p value of 0.1 or less were used as cut-offs for inclusion in this table. For the complete dataset, see Table S1.

the degree of endoplasmic reticulum (ER) stress (Inácio et al., 2015; Kaushansky and Kappe, 2015), and regulation of an extensive network of kinases (Arang et al., 2017; Prudêncio et al., 2008; Ruivo et al., 2016). Interestingly, a large portion of the hepatocyte kinome regulates LS infection (Arang et al., 2017), suggesting that phosphosignaling in the cell might be globally altered in the context of infection. Consistent with this hypothesis, a variety of signaling pathways are disrupted by *Plasmodium* infection on the transcriptional, protein, and post-translational levels (Albuquerque et al., 2009; Kaushansky et al., 2013; Posfai et al., 2018). However, the extent to which the parasite manipulates its host environment remains largely unexplored, and the mechanisms for how the parasite interacts directly with the signaling milieu remains poorly defined.

RESULTS AND DISCUSSION

Reverse Phase Protein Arrays Identify Cellular Disruptions in Susceptible Hepatocytes

We reasoned that a systematic evaluation of hepatocytes that exhibited differential susceptibility to infection might provide insight into conserved hepatocyte factors that regulate *Plasmodium* LS infection. Since hepatocytes isolated from BALB/cJ mice are less susceptible to infection than hepatocytes isolated from BALB/cByJ mice (Kaushansky et al., 2015a), and hepatocytes with elevated ploidy exhibit higher susceptibility to infection (Austin et al., 2014), we chose to compare both populations of differentially susceptible hepatocytes to identify factors that control LS infection. A limited set of transcriptional differences between hepatocytes of different susceptibilities, both polyploid (Lu et al., 2007) and BALB/c substrain (Kaushansky et al., 2015a), have been identified. However, mRNA is not always an accurate readout for protein and post-translational changes, and differences in the proteomes of BALB/cJ and BALB/cByJ mice or diploid and polyploid hepatocytes have not been characterized. To assess differences between these hepatocyte populations, we chose to use reverse phase protein microarrays (RPPAs), which enable broad but targeted interrogations of changes on the protein and post-translational levels (Sevecka et al., 2011) using cellular lysates deposited in nanoliter droplets on nitrocellulose-coated glass slides. Levels of specific proteins or their post-translational modifications can be detected by probing the printed lysates with a panel of validated antibodies (Kaushansky et al., 2013; Paweletz et al., 2001; Sevecka et al., 2011). This approach allows the analysis of up to hundreds of proteins and post-translational modifications in parallel (Paweletz et al., 2001; Sevecka et al., 2011).

To investigate the molecular differences between polyploid and diploid hepatocytes, and between BALB/cByJ and BALB/cJ livers, we probed RPPAs derived from high-susceptibility (8n hepatocytes and BALB/cByJ livers) and low-susceptibility (2n hepatocytes and BALB/cJ livers) populations with 62 antibodies that target proteins involved in cellular outcomes previously implicated in *Plasmodium* infection. These included regulators of survival, apoptosis, autophagy, cell proliferation, and cell-cycle control (Table S1).

Protein lysates were obtained from 8n and 2n primary mouse hepatocytes (BALB/cAnN) and from BALB/cJ and BALB/cByJ mouse livers. RPPAs were fabricated using a contact microarrayer, which served to deposit lysates onto nitrocellulose pads. Arrays were then probed with antibodies to obtain quantitative information on changes in host cell total or modified protein abundance. In addition to the protein or post-translational modification of interest, each array was also probed with an antibody against β-actin, which was used as a surrogate for total protein quantity. The signal from the antibody of interest was normalized to the signal from β-actin (Figures 1A and 1B).

Several proteins were significantly upregulated in BALB/cByJ livers (Figure 1; Table 1). Of these differentially regulated proteins and post-translational modifications, only one was significantly elevated in both 8n cells and BALB/cByJ livers—ribosomal

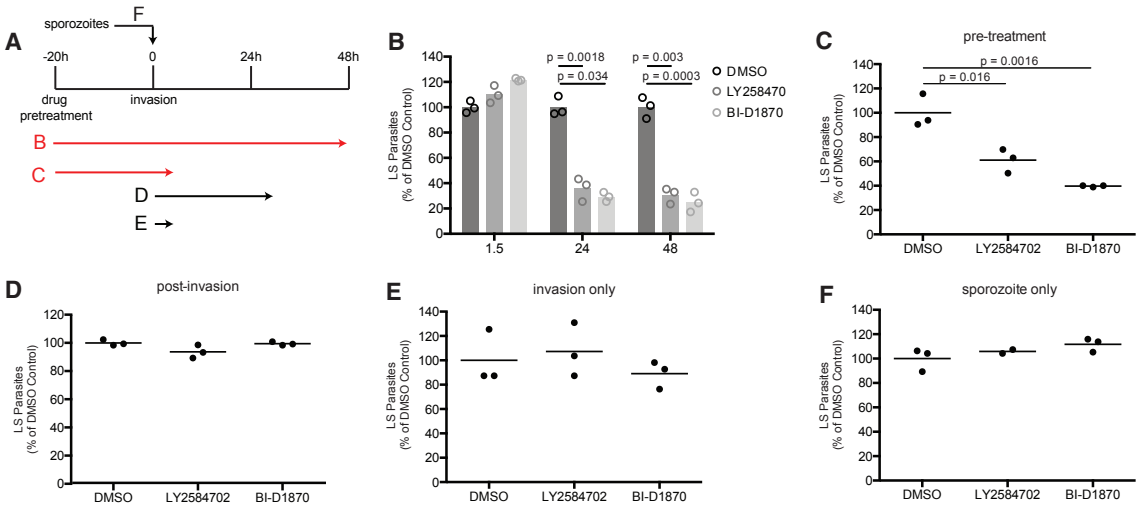

Figure 2. Pre-treatment with S6 Kinase Inhibitors Reduces LS Burden

(A) Schematic showing timing and duration of inhibitor treatment for experiments in (B)–(F). Treatment regimes indicated in red reduced LS infection.

(B) Hepa1-6 cells were pre-treated with S6K inhibitor BI-D1870 (1 μM) or LY2584702 (100 nM) for 22 h before and after infection with *P. yoelii* sporozoites. Cells were collected at 90 min, 24 h, and 48 h post-infection (hpi), and infection levels were measured by flow cytometry (90 min) or fluorescence microscopy (24 h and 48 h).

(C) Cells were treated with inhibitors for 22 h prior to infection and through invasion. Cells were fixed 24 hpi, and parasites were quantified by fluorescence microscopy.

(D) Cells were treated with inhibitors after invasion. Cells were fixed 24 hpi, and parasites were quantified by fluorescence microscopy.

(E) Cells were simultaneously treated with inhibitors and infected with *P. yoelii* sporozoites for 90 min, after which cells were washed. Cells were fixed 24 hpi, and parasites were quantified by fluorescent microscopy.

(F) Sporozoites were incubated with inhibitors and then washed before being added to untreated cells. Cells were fixed 24 hpi, and parasites were quantified by fluorescence microscopy. Data were assessed statistically by Student's t test. Data shown are from one of three biological replicates (see Table S2 for data from other biological replicates). Each point represents a technical replicate.

protein S6 (RPS6) phosphorylated on serine residues 235 and 236 (p-RPS6). To verify these findings, we evaluated levels of p-RPS6 in hepatocytes that differ in level of ploidy by flow cytometry and levels of p-RPS6 in BALB/cJ and BALB/cByJ livers via western blot (Figure S1). We found elevated levels of p-RPS6 in both BALB/cByJ livers and in Hepa 1-6 cells with high DNA content.

Small Molecule Inhibition of p-RPS6 prior to Infection Decreases Parasite Burden *In Vitro* and *In Vivo*

RPS6 is an essential part of the 40S subunit of the eukaryotic ribosome (Gressner and Wool, 1974). It is phosphorylated on five serine residues (Bandi et al., 1993; Krieg et al., 1988) through the activation of two central cell signaling pathways: the AKT/PI3K (phosphoinositol-3-kinase) pathway (Wettenhall et al., 1992) and the MEK/ERK mitogen-activated protein kinase (MAPK) pathway (Pende et al., 2004). RPS6 phosphorylation is largely regulated by the activity of two kinases: p70 S6 kinase (P70S6K) and p90 RSK kinase (P90S6K), both of which phosphorylate RPS6 on Ser235/236. RPS6 phosphorylation has been linked to cell size and proliferation (Pende et al., 2000; Ruvinsky et al., 2005), clearance of apoptotic cells (Jeon et al., 2008), and protection against DNA damage in cancerous cells (Khalaileh et al., 2013; Wittenberg et al., 2016). RPS6 has also been linked to regulation of free amino-acid levels (Ruvinsky and Meyuhas, 2006), glucose homeostasis (Pende et al., 2000; Ruvinsky et al., 2005), and lipid biosynthesis (Calvisi et al., 2011), all of which are important for parasite growth (Itani et al., 2014; Itoe et al., 2014; Meireles et al., 2017).

To determine whether phosphorylation of RPS6 has functional consequences for *Plasmodium* LS infection, we treated Hepa1-6 cells with BI-D1870, a P90S6K inhibitor (Sapkota et al., 2007), or LY2584702, an inhibitor of all P70S6K isoforms (Tolcher et al., 2014), for 20 h before infection with *P. yoelii* sporozoites and then throughout the infection. Pre-treatment with LY2584702 decreased the phosphorylation of RPS6 in uninfected cells, both at basal levels and in the context of insulin treatment (Figures S2A and S2B). BI-D1870, however, only reduced RPS6 phosphorylation modestly in the context of insulin treatment (Figures S2A and S2B). Treatment with either inhibitor did not impact host cell viability after 24 or 48 h (Figure S2C). Ninety minutes after *P. yoelii* infection, there was no significant difference in infection rate (Figure 2B). However, at both 24 and 48 h post-infection (hpi), each inhibitor significantly lowered LS numbers (Figure 2B). These data are consistent with a model where RPS6 regulates maintenance of *Plasmodium* LS infection after initial invasion. To better characterize when inhibition of RPS6 influences the survival of LS parasites, we treated cells at various time points throughout the infection process (Figure 2A). Drug treatment of cells from 20 h before infection through invasion significantly reduced LS burden at 24 hpi (Figure 2C). Adding inhibitors immediately after invasion (Figure 2D) or during invasion

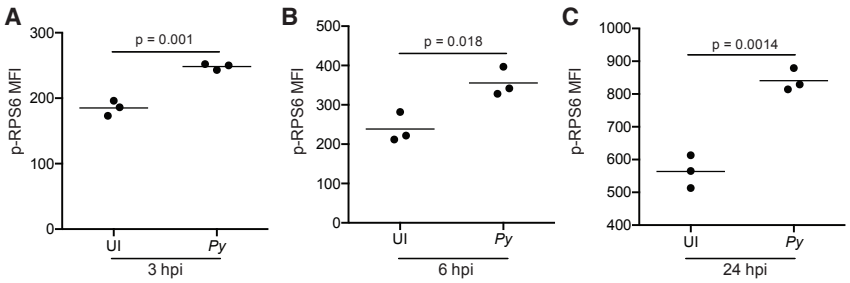

Figure 3. Phosphorylation of RPS6 Is Increased in Infected Hepatocytes

(A–C) Hepa1-6 cells were infected with *P. yoelii* sporozoites and collected at (A) 3, (B) 6, and (C) 24 hpi. p-RPS6 was quantified by flow cytometry in infected and uninfected cells, sorted by *Py*CSP staining. Data were assessed statistically by Student's t test. Data shown are from one of three biological replicates (see Table S2 for data from other biological replicates). Each point represents a technical replicate.

(Figure 2E) did not have any effect on infection at 24 h. Finally, incubation of sporozoites with inhibitors before adding them to cells had no effect on LS burden after 24 h (Figure 2F), suggesting that the inhibitors are not acting directly on the parasite. Pretreatment of cells with insulin, which stimulates phosphorylation of RPS6 (Figures S2D and S2E), increased sporozoite invasion levels after 90 min (Figure S2F). These data are consistent with the hypothesis that p-RPS6, or a process regulated by or in parallel with p-RPS6, is important for the selection of cells that are hospitable for maintenance of infection. Due to the potential for off-target effects of BI-D1870 (Neise et al., 2013; Roffé et al., 2015), we used short hairpin RNAs (shRNAs) to knock down P90S6K and then measured LS burden after 24 h. Knockdown of P90S6K by 85% reduced LS burden in Hepa1-6 cells by an average of 25% (Figures S3A and S3B). P90S6K knockdown did not reduce cell viability compared to scramble controls (Figure S3C). We were unable to generate stable hepatocyte lines upon prolonged knockdown of P70S6K.

Finally, we assessed the impact of RPS6 phosphorylation on *Plasmodium* infection *in vivo*. We treated mice with BI-D1870 or LY2584702 for 24 h and then infected them with *P. yoelii* sporozoites expressing a GFP-luciferase fusion protein (Miller et al., 2014) by intravenous injection. Treatment with each inhibitor was continued daily until the end of the experiment. Animals were injected with D-luciferin, which allowed LS burden to be monitored by bioluminescent *in vivo* imaging at 44 h after infection. At this time, livers were also harvested for histological analysis. Mice treated with LY2584702 exhibited significantly lower luciferase signal when compared to the vehicle control. In contrast, the administration of BI-D1870 had no effect (Figure S3E). The difference of activity observed in BI-D1870 *in vitro* and *in vivo* could originate from a multitude of factors. First, the bioavailability, pharmacokinetics, or off-target effects of the compound *in vivo* may alter its activity. Moreover, transformed Hepa1-6 cells *in vitro* may exhibit altered responses to primary hepatocytes found *in vivo*. Microscopic investigation of LS parasite burden demonstrated that treatment with neither BI-D1870 nor LY2584702 affected the size of parasites (Figure S3F), suggesting that RPS6 acts to curtail parasite infection by eliminating infected hepatocytes or by eliminating whole parasites within infected hepatocytes, rather than diminishing the growth of LS parasites.

RPS6 Activation in Infected Hepatocytes

Considering the absence of effect of p-RPS6 inhibition post-invasion, we asked whether p-RPS6 levels are elevated in infected cells. Increased phosphorylation of RPS6 has been seen in the context of infection with several other pathogens (Bell et al., 2017; Jakubowicz and Leader, 1987), including *Toxoplasma gondii* (Wang et al., 2009). In *T. gondii*-infected cells, p-RPS6 levels are elevated from 2 through 24 hpi. It has been proposed that this is due to the activity of mammalian target of rapamycin (mTOR), which signals through P70S6K and is localized to the parasitophorous vacuole (Wang et al., 2009). We infected Hepa1-6 cells with *P. yoelii* sporozoites and measured levels of p-RPS6 in infected and uninfected cells 3, 6, and 24 hpi. Infected cells exhibited significantly elevated levels of p-RPS6 compared to uninfected cells at all time points (Figure 3; Figure S4D). In contrast, cells mock-treated with material from uninfected mosquito salivary glands did not exhibit altered p-RPS6 levels (Figure S4A). We also observed higher levels of total RPS6 protein in *P. yoelii*-infected cells 24 hpi (Figure S4E). Due to the selective nature of *Plasmodium* sporozoite invasion, the elevated levels of p-RPS6 observed in infected cells could be due to invasion of hepatocytes that maintain high levels of p-RPS6 or to parasite perturbation of RPS6 expression and phosphorylation.

To better understand how levels of p-RPS6 are maintained in infected cells, we asked whether phosphorylation of RPS6 is regulated by the canonical signaling pathway involving phosphorylation of AKT and P70S6K in infected cells (Figure 4A). In response to growth factor stimuli such as insulin, phosphorylation of the insulin receptor leads to the recruitment of adaptor proteins, which activate PI3K and lead to the phosphorylation of AKT. Activation of AKT promotes the phosphorylation of P70S6K, which, in turn, phosphorylates RPS6 (Figure 4A) (reviewed in Meyuhas, 2015; Tavares et al., 2015). To evaluate whether elevated p-RPS6 resulted from this canonical signaling cascade, we again used RPPA. We treated cells with insulin and collected protein lysates at 5 separate time points between 3 and 48 hpi. Lysates were printed on nitrocellulose pads and probed with antibodies against p-AKT (pThr308), p-P70S6K (pThr389), and p-RPS6 (pSer235/236) to obtain quantitative information on changes in phosphorylated protein abundance. Linearity of protein detection by RPPA with these antibodies was assessed by comparing the signal from each antibody with that obtained by western blot. Each antibody exhibited a linear relationship between signals obtained by western blot and by RPPA (Figure S5).

We next assessed the relationship between different components of the pathway. We reasoned that signaling through the p-AKT/p-P70S6K/p-RPS6 axis would result in tightly correlated values of each phosphorylation site. Indeed, when we stimulated cells with insulin and lysed them between 3 and 48 hpi, we see

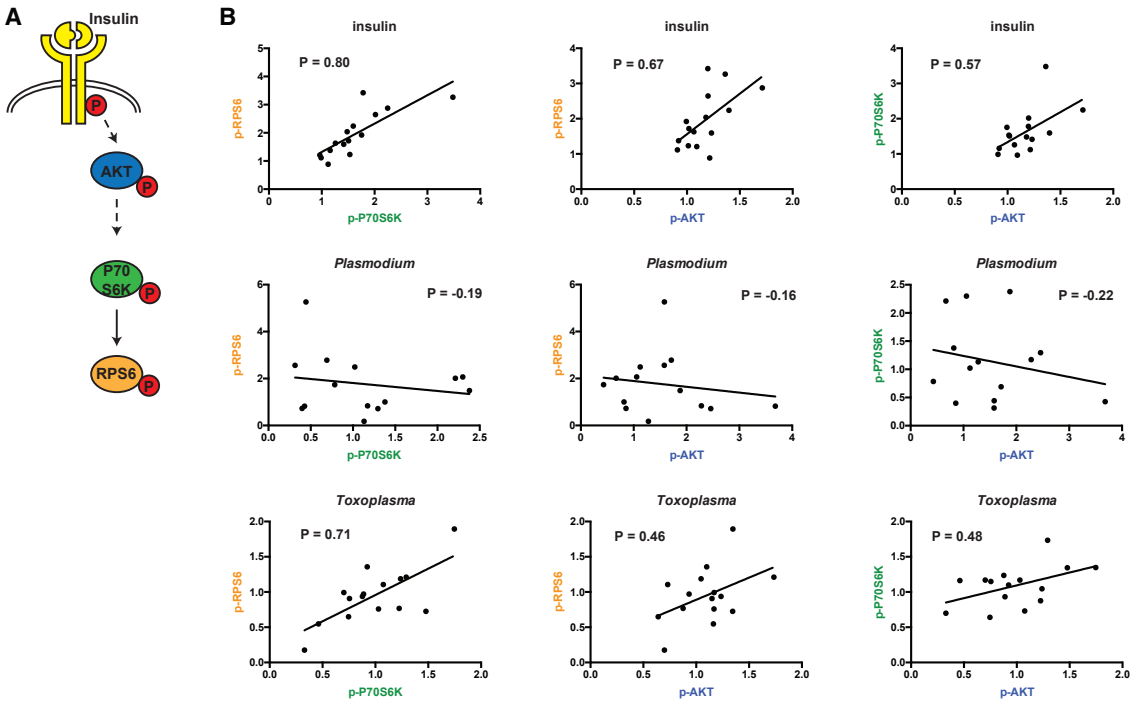

Figure 4. *Plasmodium* Infection Alters Correlation between Members of the AKT/P70S6K/RPS6 Cascade

(A) Schematic of canonical signaling pathway leading from insulin stimulation to phosphorylation of RPS6.

(B) Cells were treated with insulin or infected with *P. yoelii* or *T. gondii* and collected over a time course from 3 to 48 h (n = 3). Levels of p-AKT, p-P70S6K, and p-RPS6 were measured by RPPA. Signal from each antibody of interest was normalized to β-actin. Fold change in RPPA signal between treated and non-treated or infected and uninfected cells is plotted for each antibody pair. Each point represents a single sample from a single time point. Pearson values (P) were calculated as a measure of correlation between levels of each phosphorylated protein.

See also Table S2.

correlations between each pairwise combination of p-AKT, p-P70S6K, and p-RPS6 (Figure 4B). This is consistent with the well-established model that these kinases act within the same signal transduction cascade.

While insulin treatment is a simple and common cell stimulation, the infection of any vacuole-contained intracellular pathogen might alter signaling in both canonical and surprising ways. To determine whether the associations across this signal transduction cascade are conserved in the context of *Plasmodium* infection, we infected Hepa1-6 cells with GFP-expressing *P. yoelii* sporozoites and collected infected samples at 3, 6, 12, 24, and 48 h after infection by fluorescence-activated cell sorting (FACS). As a control, we collected uninfected cells from the same infected well. We lysed each population of cells and printed the lysates on nitrocellulose-coated glass slides for use in the RPPA. Slides were probed, as described earlier, with antibodies against p-AKT (pThr308), p-P70S6K (pThr389), and p-RPS6 (pSer235/236). Interestingly, in infected cells, phosphorylation of AKT, P70S6K, and RPS6 no longer appeared to be correlated (Figure 4B), suggesting that the canonical relationships between molecules within this signaling cascade are disrupted in *Plasmodium*-infected cells. The lack of correlation between p-P70S6K and p-RPS6 is particularly striking, as RPS6 is a substrate of P70S6K (Ruvinsky and Meyuhas, 2006).

One might presume that any pathogen that perturbs levels of p-RPS6 may exhibit altered associations between components of the p-AKT/p-P70S6K/p-RPS6 cascade. To test this hypothesis, we infected Hepa1-6 cells with the related apicomplexan parasite *Toxoplasma gondii*, which also resides within a vacuole inside the host cell, and collected samples at 3, 6, 12, 24, and 48 hpi. We then deposited these lysates on nitrocellulose-coated glass slides and evaluated levels of p-AKT, p-P70S6K, and p-RPS6 by RPPA. In *T. gondii*-infected cells, as in insulin-stimulated cells, we observed a correlation between levels of p-RPS6 and p-P70S6K (Figure 4C). Thus, the disruption of association between members of this signaling pathway is not the result of a non-specific effect of any intracellular apicomplexan and might be unique to *Plasmodium* infection.

RPS6 Is Not Phosphorylated in Response to Insulin in *Plasmodium*-Infected Cells

To examine the level of p-RPS6 on the single cell level, and without the delay caused by sorting infected cells, we used flow cytometry to measure the effect of infection on insulin-induced p-RPS6. Hepa1-6 cells were infected with *P. yoelii* or *T. gondii.* After 24 h, infected (or uninfected) cells were treated with insulin for 30 min before fixation. Cells were then processed for flow cytometry. As seen previously (Figure 3), *P. yoelii*-infected cells exhibited elevated levels of p-RPS6 at 24 h (Figure 5A).

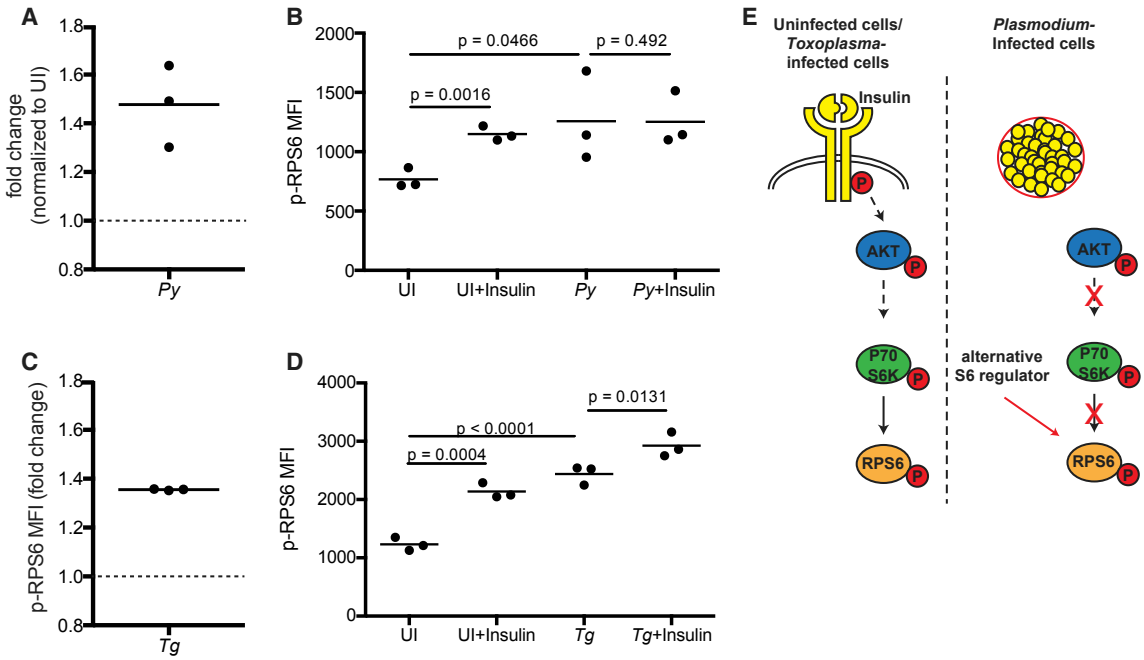

Figure 5. *Plasmodium* Infection Prevents Phosphorylation of RPS6 in Response to Insulin Treatment

(A) Fold change in p-RPS6 mean fluorescence intensity (MFI) between uninfected (UI) and *P. yoelii*-infected Hepa1-6 cells 24 hpi. Each point represents a biological replicate.

(B) p-RPS6 MFI of Hepa1-6 cells that were either uninfected or infected with *P. yoelii* sporozoites for 24 h before treatment with insulin or a diluent control for 30 min. Data shown are from one of three biological replicates (see Table S2 for data from other biological replicates). Each point is a technical replicate.

(C) Fold change in p-RPS6 mean fluorescence intensity (MFI) between uninfected and *T. gondii*-infected Hepa1-6 cells 24 hpi. Each point represents a biological replicate.

(D) p-RPS6 MFI of Hepa1-6 cells that were uninfected or infected with *T. gondii* for 24 h before treatment with insulin for 30 min. Data shown are from one of three biological replicates (see Table S2 for data from other biological replicates). Each point is a technical replicate. Data were assessed statistically by Student's t test.

(E) Schematic of proposed signaling pathways leading to phosphorylation of RPS6 in uninfected, *Toxoplasma*-infected, and *Plasmodium*-infected cells.

T. gondii-infected cells also had similarly increased p-RPS6 levels at 24 h (Figure 5C), consistent with what has been seen in other cell types (Wang et al., 2009). Insulin-treated uninfected cells had significantly higher levels of p-RPS6 than non-treated cells (Figure 5D). However, in *P. yoelii*-infected cells, insulin treatment did not significantly increase p-RPS6 (Figure 5B). In comparison, insulin treatment of *T. gondii*-infected cells significantly increased p-RPS6 levels compared to infected but untreated cells (Figure 5D). Mock infections for either pathogen did not alter p-RPS6 levels or prevent an increase in response to insulin (Figures S4B and S4C).

The additive effect of infection and insulin treatment that we observed during *T. gondii* infection suggests that AKT/P70S6K/RPS6 signaling remains intact during *T. gondii* infection. In contrast, our data are consistent with a model where AKT/P70S6K/RPS6 signaling loses its normal connectivity in *P. yoelii*-infected cells, either due to parasite manipulation or pre-selection of hepatocytes with alternate p-RPS6 regulation by sporozoites. The lack of response to insulin in *P. yoelii*-infected cells is unlikely to be due to saturation of RPS6 phosphorylation—since we observed similar levels of RPS6 phosphorylation in response to *T. gondii* (Figures 5A and 5C) and increased total RPS6 levels in *P. yoelii*-infected cells (Figure S4E)—but instead, due to the nature of the infection, or the infected cell, itself. Taken together, the data are consistent with a model where *Plasmodium* infection activates RPS6 while simultaneously disrupting the ability of P70S6K to do so (Figure 5E). Supporting this model is our finding that levels of p-P70S6K and p-RPS6 are not correlated during *Plasmodium* infection (Figure 4) and the observation that insulin treatment does not lead to the activation of p-RPS6 during *Plasmodium* infection (Figure 5B). Finally, this model is consistent with the observed effect of the P70S6K inhibitor, LY2584702. Inhibition of P70S6K before infection and rewiring of signaling networks by the parasite (Figures 2B and 2C)—but not after infection (Figure 2D) when, we hypothesize, parasites have already altered the signaling network—decreases the number of LS-infected hepatocytes. The mechanism by which *Plasmodium* may exert control over its host hepatocyte remains unknown.

Alternatively, *Plasmodium* sporozoites may preferentially infect hepatocytes that have higher basal levels of RPS6 phosphorylation and altered connectivity between P70S6K and RPS6 and, thus, are insensitive to insulin stimulation. Under this scenario, pre-treatment with S6K inhibitors may prevent sporozoites from invading the proper host cells, leading to infection failure and the reduction in LS burden we see by 24 hpi.

Plasmodium LS infection remodels the host hepatocyte, including physical and transcriptional changes (Albuquerque et al., 2009; Kaushansky et al., 2013; Zuck et al., 2017; Posfai

et al., 2018). Optimal maintenance of LS infection is dependent on the activity of a large number of host kinases regulating processes such as cytoskeletal organization and apoptosis (Arang et al., 2017). These observations are consistent with the hypothesis that the parasite rewires a portion of host cell signaling in a manner that disrupts canonical signal transduction cascades. Our observation that the insulin/AKT/RPS6 pathway, which has been described across metazoans, is disrupted in *Plasmodium*-infected cells suggests that the regulation of even well-conserved pathways may be heterogeneous across individual cells and may be susceptible to being coopted by the parasite. RPS6 regulates a plethora of host cell processes that may regulate successful LS infection, including cell growth and glucose and lipid availability. *Plasmodium* manipulation of AMPK phosphorylation, a major regulator of nutrient homeostasis, during LS infection (Ruivo et al., 2016) and a role for host diet in influencing parasite survival in the liver (Zuzarte-Luís et al., 2017) were also recently described, suggesting that the metabolic state within the liver is crucial for determining infection outcome. By developing within a cell with high RPS6 phosphorylation, disconnected from canonical upstream regulators, *Plasmodium* parasites may be ensuring an environment favorable to their development, either through selection or manipulation.

The extent of pathway alterations in hepatocytes during *Plasmodium* infection, as well as the portion of these alterations that are mediated by direct contact with parasite molecules, remains to be explored. By gaining a better understanding of what host proteins are essential for LS infection, and how signaling within hepatocytes is altered by infection, we will elucidate the process by which the host cell environment is selected for, and manipulated by, *Plasmodium* and identify targets for intervention.

STAR★METHODS

Detailed methods are provided in the online version of this paper and include the following:

- KEY RESOURCES TABLE
- CONTACT FOR REAGENT AND RESOURCE SHARING
- EXPERIMENTAL MODEL AND SUBJECT DETAILS
  - Cell lines and cell culture
  - Experimental animals
  - Mosquito rearing and sporozoite production
  - *T. gondii* production and infection
- METHOD DETAILS
  - Small molecule treatment
  - Hepatocyte isolation and processing
  - Reverse phase protein microarray
  - *In vitro* immunofluorescence and quantification
  - Flow cytometry of infected and uninfected cells
  - Immunofluorescence Microscopy
  - Western blotting
  - *In vivo* treatment and infection
  - *In vivo* bioluminescent imaging of liver-stage development
- QUANTIFICATION AND STATISTICAL ANALYSIS

SUPPLEMENTAL INFORMATION

Supplemental Information can be found with this article online at https://doi.org/10.1016/j.celrep.2019.02.085.

ACKNOWLEDGMENTS

We thank Photini Sinnis and Fidel Zavala for the *P. yoelii* Hsp70 antisera and Marilyn Parsons for the *T. gondii* strain. We thank the Center for Infectious Disease Research vivarium staff for their work with mice. All work was done according to Institutional Animal Care and Use Committee (IACUC) procedures and protocols. This work was supported by NIH grants R01GM101183 (to A.K.), 1K99/R00AI111785 (to A.K.), T32 Postdoctoral Fellowship AI07509 (to E.K.K.G.), and P41 GM109824 (to J.D.A.). F.D.M. is a postdoctoral fellow of the Canadian Institutes of Health Research. L.S.A. was supported by the Department of Defense NDSEG fellowship.

AUTHOR CONTRIBUTIONS

E.K.K.G., L.S.A., N.A., K.V., H.S.K., and F.D.M. performed experiments. A.K., J.D.A., and S.H.I.K. supervised the research. E.K.K.G., L.S.A., and A.K. wrote the paper, with input from all other authors.

DECLARATION OF INTERESTS

The authors declare no competing interests.

Received: May 8, 2018
Revised: October 11, 2018
Accepted: February 21, 2019
Published: March 19, 2019

REFERENCES

Albuquerque, S.S., Carret, C., Grosso, A.R., Tarun, A.S., Peng, X., Kappe, S.H., Prudêncio, M., and Mota, M.M. (2009). Host cell transcriptional profiling during malaria liver stage infection reveals a coordinated and sequential set of biological events. BMC Genomics *10*, 270.

Arang, N., Kain, H.S., Glennon, E.K., Bello, T., Dudgeon, D.R., Walter, E.N.F., Gujral, T.S., and Kaushansky, A. (2017). Identifying host regulators and inhibitors of liver stage malaria infection using kinase activity profiles. Nat. Commun. *8*, 1232.

Austin, L.S., Kaushansky, A., and Kappe, S.H. (2014). Susceptibility to *Plasmodium* liver stage infection is altered by hepatocyte polyploidy. Cell. Microbiol. *16*, 784–795.

Bandi, H.R., Ferrari, S., Krieg, J., Meyer, H.E., and Thomas, G. (1993). Identification of 40 S ribosomal protein S6 phosphorylation sites in Swiss mouse 3T3 fibroblasts stimulated with serum. J. Biol. Chem. *268*, 4530–4533.

Bell, T.M., Espina, V., Senina, S., Woodson, C., Brahms, A., Carey, B., Lin, S.C., Lundberg, L., Pinkham, C., Baer, A., et al. (2017). Rapamycin modulation of p70 S6 kinase signaling inhibits Rift Valley fever virus pathogenesis. Antiviral Res. *143*, 162–175.

Calvisi, D.F., Wang, C., Ho, C., Ladu, S., Lee, S.A., Mattu, S., Destefanis, G., Delogu, S., Zimmermann, A., Ericsson, J., et al. (2011). Increased lipogenesis, induced by AKT-mTORC1-RPS6 signaling, promotes development of human hepatocellular carcinoma. Gastroenterology *140*, 1071–1083.

Douglass, A.N., Kain, H.S., Abdullahi, M., Arang, N., Austin, L.S., Mikolajczak, S.A., Billman, Z.P., Hume, J.C., Murphy, S.C., Kappe, S.H., et al. (2015). Host-based prophylaxis successfully targets liver stage malaria parasites. Mol. Ther. *23*, 857–865.

Gressner, A.M., and Wool, I.G. (1974). The phosphorylation of liver ribosomal proteins in vivo. Evidence that only a single small subunit protein (S6) is phosphorylated. J. Biol. Chem. *249*, 6917–6925.

Gueirard, P., Tavares, J., Thiberge, S., Bernex, F., Ishino, T., Milon, G., Franke-Fayard, B., Janse, C.J., Ménard, R., and Amino, R. (2010). Development of the

malaria parasite in the skin of the mammalian host. Proc. Natl. Acad. Sci. USA *107*, 18640–18645.

Inácio, P., Zuzarte-Luís, V., Ruivo, M.T., Falkard, B., Nagaraj, N., Rooijers, K., Mann, M., Mair, G., Fidock, D.A., and Mota, M.M. (2015). Parasite-induced ER stress response in hepatocytes facilitates *Plasmodium* liver stage infection. EMBO Rep. *16*, 955–964.

Itani, S., Torii, M., and Ishino, T. (2014). D-glucose concentration is the key factor facilitating liver stage maturation of *Plasmodium*. Parasitol. Int. *63*, 584–590.

Itoe, M.A., Sampaio, J.L., Cabal, G.G., Real, E., Zuzarte-Luis, V., March, S., Bhatia, S.N., Frischknecht, F., Thiele, C., Shevchenko, A., and Mota, M.M. (2014). Host cell phosphatidylcholine is a key mediator of malaria parasite survival during liver stage infection. Cell Host Microbe *16*, 778–786.

Jakubowicz, T., and Leader, D.P. (1987). Activation of a ribosomal protein S6 kinase in mouse fibroblasts during infection with herpesvirus. Eur. J. Biochem. *168*, 371–376.

Jeon, Y.J., Kim, I.K., Hong, S.H., Nan, H., Kim, H.J., Lee, H.J., Masuda, E.S., Meyuhas, O., Oh, B.H., and Jung, Y.K. (2008). Ribosomal protein S6 is a selective mediator of TRAIL-apoptotic signaling. Oncogene *27*, 4344–4352.

Kaushansky, A., and Kappe, S.H. (2015). Host ER stress during malaria parasite infection. EMBO Rep. *16*, 883–884.

Kaushansky, A., Ye, A.S., Austin, L.S., Mikolajczak, S.A., Vaughan, A.M., Camargo, N., Metzger, P.G., Douglass, A.N., MacBeath, G., and Kappe, S.H. (2013). Suppression of host p53 is critical for *Plasmodium* liver-stage infection. Cell Rep. *3*, 630–637.

Kaushansky, A., Austin, L.S., Mikolajczak, S.A., Lo, F.Y., Miller, J.L., Douglass, A.N., Arang, N., Vaughan, A.M., Gardner, M.J., and Kappe, S.H. (2015a). Susceptibility to *Plasmodium yoelii* preerythrocytic infection in BALB/c substrains is determined at the point of hepatocyte invasion. Infect. Immun. *83*, 39–47.

Kaushansky, A., Douglass, A.N., Arang, N., Vigdorovich, V., Dambrauskas, N., Kain, H.S., Austin, L.S., Sather, D.N., and Kappe, S.H. (2015b). Malaria parasites target the hepatocyte receptor EphA2 for successful host infection. Science *350*, 1089–1092.

Khalaileh, A., Dreazen, A., Khatib, A., Apel, R., Swisa, A., Kidess-Bassir, N., Maitra, A., Meyuhas, O., Dor, Y., and Zamir, G. (2013). Phosphorylation of ribosomal protein S6 attenuates DNA damage and tumor suppression during development of pancreatic cancer. Cancer Res. *73*, 1811–1820.

Khan, Z.M., and Vanderberg, J.P. (1991). Role of host cellular response in differential susceptibility of nonimmunized BALB/c mice to Plasmodium berghei and *Plasmodium yoelii* sporozoites. Infect. Immun. *59*, 2529–2534.

Krieg, J., Hofsteenge, J., and Thomas, G. (1988). Identification of the 40 S ribosomal protein S6 phosphorylation sites induced by cycloheximide. J. Biol. Chem. *263*, 11473–11477.

Liehl, P., Zuzarte-Luís, V., Chan, J., Zillinger, T., Baptista, F., Carapau, D., Konert, M., Hanson, K.K., Carret, C., Lassnig, C., et al. (2014). Host-cell sensors for *Plasmodium* activate innate immunity against liver-stage infection. Nat. Med. *20*, 47–53.

Liehl, P., Meireles, P., Albuquerque, I.S., Pinkevych, M., Baptista, F., Mota, M.M., Davenport, M.P., and Prudêncio, M. (2015). Innate immunity induced by *Plasmodium* liver infection inhibits malaria reinfections. Infect. Immun. *83*, 1172–1180.

Lu, P., Prost, S., Caldwell, H., Tugwood, J.D., Betton, G.R., and Harrison, D.J. (2007). Microarray analysis of gene expression of mouse hepatocytes of different ploidy. Mamm. Genome *18*, 617–626.

March, S., Ng, S., Velmurugan, S., Galstian, A., Shan, J., Logan, D.J., Carpenter, A.E., Thomas, D., Sim, B.K., Mota, M.M., et al. (2013). A microscale human liver platform that supports the hepatic stages of *Plasmodium falciparum* and *vivax*. Cell Host Microbe *14*, 104–115.

Meireles, P., Mendes, A.M., Aroeira, R.I., Mounce, B.C., Vignuzzi, M., Staines, H.M., and Prudêncio, M. (2017). Uptake and metabolism of arginine impact *Plasmodium* development in the liver. Sci. Rep. *7*, 4072.

Meyuhas, O. (2015). Ribosomal protein S6 phosphorylation: four decades of research. Int. Rev. Cell Mol. Biol. *320*, 41–73.

Miller, J.L., Murray, S., Vaughan, A.M., Harupa, A., Sack, B., Baldwin, M., Crispe, I.N., and Kappe, S.H. (2013). Quantitative bioluminescent imaging of pre-erythrocytic malaria parasite infection using luciferase-expressing *Plasmodium yoelii*. PLoS ONE *8*, e60820.

Miller, J.L., Sack, B.K., Baldwin, M., Vaughan, A.M., and Kappe, S.H. (2014). Interferon-mediated innate immune responses against malaria parasite liver stages. Cell Rep. *7*, 436–447.

Neise, D., Sohn, D., Stefanski, A., Goto, H., Inagaki, M., Wesselborg, S., Budach, W., Stühler, K., and Jänicke, R.U. (2013). The p90 ribosomal S6 kinase (RSK) inhibitor BI-D1870 prevents gamma irradiation-induced apoptosis and mediates senescence via RSK- and p53-independent accumulation of p21WAF1/CIP1. Cell Death Dis. *4*, e859.

Øvrebø, J.I., and Edgar, B.A. (2018). Polyploidy in tissue homeostasis and regeneration. Development *145*, dev156034.

Paweletz, C.P., Charboneau, L., Bichsel, V.E., Simone, N.L., Chen, T., Gillespie, J.W., Emmert-Buck, M.R., Roth, M.J., Petricoin, E.F., III, and Liotta, L.A. (2001). Reverse phase protein microarrays which capture disease progression show activation of pro-survival pathways at the cancer invasion front. Oncogene *20*, 1981–1989.

Pende, M., Kozma, S.C., Jaquet, M., Oorschot, V., Burcelin, R., Le Marchand-Brustel, Y., Klumperman, J., Thorens, B., and Thomas, G. (2000). Hypoinsulinaemia, glucose intolerance and diminished beta-cell size in S6K1-deficient mice. Nature *408*, 994–997.

Pende, M., Um, S.H., Mieulet, V., Sticker, M., Goss, V.L., Mestan, J., Mueller, M., Fumagalli, S., Kozma, S.C., and Thomas, G. (2004). S6K1(-/-)/S6K2(-/-) mice exhibit perinatal lethality and rapamycin-sensitive 5′-terminal oligopyrimidine mRNA translation and reveal a mitogen-activated protein kinase-dependent S6 kinase pathway. Mol. Cell. Biol. *24*, 3112–3124.

Posfai, D., Sylvester, K., Reddy, A., Ganley, J.G., Wirth, J., Cullen, Q.E., Dave, T., Kato, N., Dave, S.S., and Derbyshire, E.R. (2018). *Plasmodium* parasite exploits host aquaporin-3 during liver stage malaria infection. PLoS Pathog. *14*, e1007057.

Prudêncio, M., Rodrigues, C.D., Hannus, M., Martin, C., Real, E., Gonçalves, L.A., Carret, C., Dorkin, R., Röhl, I., Jahn-Hoffmann, K., et al. (2008). Kinome-wide RNAi screen implicates at least 5 host hepatocyte kinases in *Plasmodium* sporozoite infection. PLoS Pathog. *4*, e1000201.

Roffé, M., Lupinacci, F.C., Soares, L.C., Hajj, G.N., and Martins, V.R. (2015). Two widely used RSK inhibitors, BI-D1870 and SL0101, alter mTORC1 signaling in a RSK-independent manner. Cell. Signal. *27*, 1630–1642.

Ruivo, M.T.G., Vera, I.M., Sales-Dias, J., Meireles, P., Gural, N., Bhatia, S.N., Mota, M.M., and Mancio-Silva, L. (2016). Host AMPK is a modulator of *Plasmodium* liver infection. Cell Rep. *16*, 2539–2545.

Ruvinsky, I., and Meyuhas, O. (2006). Ribosomal protein S6 phosphorylation: from protein synthesis to cell size. Trends Biochem. Sci. *31*, 342–348.

Ruvinsky, I., Sharon, N., Lerer, T., Cohen, H., Stolovich-Rain, M., Nir, T., Dor, Y., Zisman, P., and Meyuhas, O. (2005). Ribosomal protein S6 phosphorylation is a determinant of cell size and glucose homeostasis. Genes Dev. *19*, 2199–2211.

Sapkota, G.P., Cummings, L., Newell, F.S., Armstrong, C., Bain, J., Frodin, M., Grauert, M., Hoffmann, M., Schnapp, G., Steegmaier, M., et al. (2007). BI-D1870 is a specific inhibitor of the p90 RSK (ribosomal S6 kinase) isoforms in vitro and in vivo. Biochem. J. *401*, 29–38.

Scheele, S., Geiger, J.A., DeRocher, A.E., Choi, R., Smith, T.R., Hulverson, M.A., Vidadala, R.S.R., Barrett, L.K., Maly, D.J., Merritt, E.A., et al. (2018). *Toxoplasma* calcium-dependent protein kinase 1 inhibitors: probing activity and resistance using cellular thermal shift assays. Antimicrob. Agents Chemother. *62*, e00051–e18.

Scheller, L.F., Wirtz, R.A., and Azad, A.F. (1994). Susceptibility of different strains of mice to hepatic infection with *Plasmodium berghei*. Infect. Immun. *62*, 4844–4847.

Sevecka, M., Wolf-Yadlin, A., and MacBeath, G. (2011). Lysate microarrays enable high-throughput, quantitative investigations of cellular signaling. Mol. Cell Proteomics *10*, M110.005363.

Silvie, O., Greco, C., Franetich, J.F., Dubart-Kupperschmitt, A., Hannoun, L., van Gemert, G.J., Sauerwein, R.W., Levy, S., Boucheix, C., Rubinstein, E., and Mazier, D. (2006). Expression of human CD81 differently affects host cell susceptibility to malaria sporozoites depending on the *Plasmodium* species. Cell. Microbiol. *8*, 1134–1146.

Sinturel, F., Gerber, A., Mauvoisin, D., Wang, J., Gatfield, D., Stubblefield, J.J., Green, C.B., Gachon, F., and Schibler, U. (2017). Diurnal oscillations in liver mass and cell size accompany ribosome assembly cycles. Cell *169*, 651–663.e14.

Tavares, M.R., Pavan, I.C., Amaral, C.L., Meneguello, L., Luchessi, A.D., and Simabuco, F.M. (2015). The S6K protein family in health and disease. Life Sci. *131*, 1–10.

Thieleke-Matos, C., Lopes da Silva, M., Cabrita-Santos, L., Portal, M.D., Rodrigues, I.P., Zuzarte-Luis, V., Ramalho, J.S., Futter, C.E., Mota, M.M., Barral, D.C., and Seabra, M.C. (2016). Host cell autophagy contributes to *Plasmodium* liver development. Cell. Microbiol. *18*, 437–450.

Tolcher, A., Goldman, J., Patnaik, A., Papadopoulos, K.P., Westwood, P., Kelly, C.S., Bumgardner, W., Sams, L., Geeganage, S., Wang, T., et al. (2014). A phase I trial of LY2584702 tosylate, a p70 S6 kinase inhibitor, in patients with advanced solid tumours. Eur. J. Cancer *50*, 867–875.

Trampuz, A., Jereb, M., Muzlovic, I., and Prabhu, R.M. (2003). Clinical review: severe malaria. Crit. Care *7*, 315–323.

Tsuji, M., Mattei, D., Nussenzweig, T.S., Eichinger, D., and Zavala, F. (1994). Demonstration of heat-shock protein 70 in the sporozoite stage of malaria parasites. Parasitol Res *80*, 16–21.

Vaughan, A.M., Aly, A.S., and Kappe, S.H. (2008). Malaria parasite pre-erythrocytic stage infection: gliding and hiding. Cell Host Microbe *4*, 209–218.

Wang, Y., Weiss, L.M., and Orlofsky, A. (2009). Intracellular parasitism with *Toxoplasma gondii* stimulates mammalian-target-of-rapamycin-dependent host cell growth despite impaired signalling to S6K1 and 4E-BP1. Cell. Microbiol. *11*, 983–1000.

Wettenhall, R.E., Erikson, E., and Maller, J.L. (1992). Ordered multisite phosphorylation of *Xenopus* ribosomal protein S6 by S6 kinase II. J. Biol. Chem. *267*, 9021–9027.

Wittenberg, A.D., Azar, S., Klochendler, A., Stolovich-Rain, M., Avraham, S., Birnbaum, L., Binder Gallimidi, A., Katz, M., Dor, Y., and Meyuhas, O. (2016). Phosphorylated ribosomal protein S6 is required for Akt-driven hyperplasia and malignant transformation, but not for hypertrophy, aneuploidy and hyperfunction of pancreatic β-cells. PLoS ONE *11*, e0149995.

Yalaoui, S., Huby, T., Franetich, J.F., Gego, A., Rametti, A., Moreau, M., Collet, X., Siau, A., van Gemert, G.J., Sauerwein, R.W., et al. (2008). Scavenger receptor BI boosts hepatocyte permissiveness to *Plasmodium* infection. Cell Host Microbe *4*, 283–292.

Zuck, M., Austin, L.S., Danziger, S.A., Aitchison, J.D., and Kaushansky, A. (2017). The promise of systems biology approaches for revealing host pathogen interactions in malaria. Front. Microbiol. *8*, 2183.

Zuzarte-Luís, V., Mello-Vieira, J., Marreiros, I.M., Liehl, P., Chora, Â.F., Carret, C.K., Carvalho, T., and Moto, M.M. (2017). Dietary alterations modulate susceptibility to Plasmodium infection. Nat. Microbiol *2*, 1600–1607.

STAR★METHODS

KEY RESOURCES TABLE

REAGENT or RESOURCE	SOURCE	IDENTIFIER
Antibodies		
AlexaFluor-647 donkey anti-rabbit	ThermoFisher	Cat# A31573; RRID:AB_2536183
AlexaFluor-555 goat anti-mouse	ThermoFisher	Cat# A21424; RRID:AB_141780
Mouse anti-*Plasmodium* HSP70	Photini Sinnis, Fidel Zavala	Tsuji et al. 1994
AlexaFluor-488 goat anti-mouse	Invitrogen	Cat# A-11001; RRID:AB_2534069
T. gondii P30 mouse monoclonal antibody	Novus Biologicals	Cat# NB100-66486; RRID:AB_965730
Rabbit anti-p-RPS6 (S235/6) antibody	Cell Signaling	Cat# 4858; RRID:AB_916156
Mouse anti-RPS6 antibody	Cell Signaling	Cat# 2317; RRID:AB_2238583
Mouse anti-B-actin antibody	Cell Signaling	Cat# 3700; RRID:AB_2242334
AlexaFluor-647 donkey anti-rabbit	Invitrogen	Cat# A-31573; RRID:AB_2536183
All primary antibodies used in lysate array	Cell Signaling	See Table S1
Chemicals, Peptides, and Recombinant Proteins		
BI-D1870	SelleckChem	S2843
LY258470	SelleckChem	S7698
ITSS	Sigma-Aldrich	11074547001
Critical Commercial Assays		
FxCycle Far Red Stain	Invitrogen	F10348
Experimental Models: Cell Lines		
Hepa1-6, mouse hepatoma cells	ATCC	Cat# CRL-1830; RRID:CVCL_0327
HFF, human foreskin fibroblasts	ATCC	Cat# SCRC-1041; RRID:CVCL_3285
Experimental Models: Organisms/Strains		
Mouse: BALB/cAnN mice, female, 6-8 weeks old	Envigo (formerly Harlan)	047
Mouse: BALB/cJ, female, 6-8 weeks old	Jackson Laboratory	000651
Mouse: BALB/cByJ, female, 6-8 weeks old	Jackson Laboratory	001026
Toxoplasma gondii RHΔHXGPRT Gra2:GFP	Marilyn Parsons	Scheele et al., 2018
Plasmodium yoelii 17XNL	BEI Resources	MRA-593
Plasmodium yoelii 17XNL GFP-Luc	Stefan Kappe	Miller et al., 2013
Oligonucleotides		
Primer for P90S6K F: CCATCACACACCACGTCAAG	https://pga.mgh.harvard.edu/primerbank/	Primer pair 4
Primer for P90S6K R: TTGCGTACCAGGAAGACTTTG	https://pga.mgh.harvard.edu/primerbank/	Primer pair 4
Recombinant DNA		
RPS6KA1 Mission shRNA	SigmaAldrich	TRCN0000022824
RPS6KA1 Mission shRNA	SigmaAldrich	TRCN0000285729
RPS6KB1 Mission shRNA	SigmaAldrich	TRCN0000022904
RPS6KB1 Mission shRNA	SigmaAldrich	TRCN0000022908
Software and Algorithms		
Living Image 3.0	PerkinElmer	n/a
Huygens Profession Software	Scientific Volume Imaging BV	n/a
FlowJo	Tree Star	n/a
Innopsis Mapix Software	https://www.innopsys.com/en/lifesciences-products/microarrays/software/mapix	n/a
GraphPad Prism 7	https://www.graphpad.com/scientific-software/prism/	n/a

CONTACT FOR REAGENT AND RESOURCE SHARING

Further information and requests for resources and reagents should be directed to the Lead Contact, Alexis Kaushansky (alexis.kaushansky@seattlechildrens.org).

EXPERIMENTAL MODEL AND SUBJECT DETAILS

Cell lines and cell culture

In vitro, Hepa1-6 cells were used for *P. yoelii* infections and western blots. Cells were maintained in Dulbecco's Modified Eagle Medium (DMEM) complete media (Cellgro), supplemented with 10% FBS (Sigma-Aldrich), 100IU/ml penicillin (Cellgro), 100mg/ml streptomycin (Cellgro), and 2.5mg/ml Fungizone (HyClone/Thermo Fisher).

Experimental animals

Female BALB/cAnN mice (6-8 weeks old) were purchased from Harlan Laboratories. Female BALB/cJ and BALB/cByJ (6-8 weeks old) were purchased from Jackson Laboratories. All mice were maintained in accordance with protocols approved by Center for Infectious Disease Research Institutional Animal Control and Use Committee (IACUC).

Mosquito rearing and sporozoite production

For *Plasmodium* sporozoite production, female 6–8-week-old Swiss Webster mice (Harlan) were injected with blood stage *P. yoelii* 17XNL or *Py*GFP-Luc (Miller et al., 2013) parasites to begin the growth cycle. Animal handling was conducted according to the Institutional Animal Care and Use Committee-approved protocols. Infected mice were used to feed female *Anopheles stephensi* mosquitoes after gametocyte exflagellation was observed. Salivary glands were dissected at days 14 or 15 post blood meal. Sporozoites were isolated by mechanical grinding of pooled salivary glands, followed by centrifugation for 2 minutes at 800 RPM and collection of supernatant.

T. gondii production and infection

T. gondii strain RHΔHXGPRT Gra2:GFP, Tub:βgal, was maintained by continual cycling through human foreskin fibroblasts (HFF). Parasites were lysed from HFFs by passing 2x through a 27-gauge needle. 1.5×10^5 parasites were used to infect 5×10^5 Hepa1-6 cells in a 24-well plate for 90 min before cells were washed and media replaced.

METHOD DETAILS

Small molecule treatment

BI-D1870 and LY2584702 (SelleckChem) were resuspended in DMSO at a stock solution of 10 mM (BI-D1870) or 1 mM (LY2584702). Stocks were diluted into cell media to 1 μM (BI-D1870) or 100 nM (LY2584702) and added to Hepa1-6 cells. Cells were treated 22 h previous to infection or immediately after infection, as indicated, and media and treatment refreshed every 24 h thereafter. Insulin-transferrin-sodium selenite (ITSS) was resuspended in water at a stock solution of 5mg/mL. Cells were treated at a final concentration of 0.5 ug/mL. Live-dead assays were performed using trypan blue staining (Sigma-Aldrich).

Hepatocyte isolation and processing

Hepatocytes were isolated from mice using a two-step perfusion *in situ*. Portal veins of anesthetized mice were cannulated with warmed perfusion buffer (1x HBSS w/o calcium, magnesium supplemented with 8 mM HEPES buffer and 0.5 mM EDTA) at low flow rate. Once cannulated, the inferior vena cava was severed to blanch the liver. The buffer flow rate was increased to 5 mL/min and allowed to perfuse for five min with occasional clamping and releasing of the vena cava to inflate the liver. The liver was then perfused with 2% collagenase II (Worthington) in collagenase buffer (HBSS supplemented with 8 mM HEPES and 0.5 mM CaCl2) for five min at 5 mL/min. The liver was then removed from the abdominal cavity and the gall bladder excised. The liver was placed in a dish of DMEM without serum and gently pushed through a 100-micron cell strainer to dissociate the hepatocytes, which were then collected with a wide-bore syringe. The liver cell suspension was centrifuged at 50x *g*, and the remaining pellet washed in DMEM without serum. This step was repeated twice until the supernatant was clear, to isolate hepatocytes from cell debris and non-parenchymal cells.

Reverse phase protein microarray

For BALB/c substrains, whole livers from BALB/cJ and BALB/cByJ mice (n = 10 per strain) were briefly rinsed in a 20 mM HEPES-KOH, pH 7.4 buffer before being plunged into liquid nitrogen and snap frozen. Frozen livers were weighed and then sequentially cryomilled under liquid nitrogen in a Retsch PM 100 planetary ball mill. The jar was cooled in liquid nitrogen in between milling cycles. An additional three cryomilling cycles of same duration were performed with twenty 10 mm stainless steel balls. Cryomilling reduces the liver to a powder of exceptional fineness with < 1 – 0.1 μm sized grindate, as judged by light microscopy. Powder was then reconstituted in SDS Lysis Buffer (2% SDS, 50 mM Tris-HCl, 5% glycerol, 5 mM EDTA, 1 mM NaF, 10 mM β-glycerophosphate,

1 mM PMSF, 1 mM activated Na_3VO_4, 1 mM DTT, 1% phosphatase inhibitor cocktail 2 (Sigma Aldrich) and 1% phosphatase inhibitor cocktail 3 (Sigma-Aldrich), 1% PhosSTOP Phosphatase Inhibitor Cocktail Tablet (Roche)), and stored at −80°C. To isolate hepatocytes of differing ploidy, livers of BALB/cAnN mice were perfused and processed as described above. Cells were stained for DNA content with Vybrant DyeCycle Orange (Invitrogen) in DMEM without serum and sorted on a BD Influx (BD Biosciences).

Custom lysate microarrays were printed using an Aushon Biosystems 2470 arrayer (Aushon Biosystems) on 16-pad nitrocellulose-coated glass slides (Grace Bio-Labs). Lysates were arrayed at 333 μM spacing using solid 110 μM pins, which resulted in an average feature diameter of 170 μM. Lysates were arrayed in quadruplicate technical replicates. Slides were then stored dry, in the dark, and at room temperature until probing. Slides were probed and quantified as previously described by Sevecka et al. (2011). Slides were washed with 0.1% Tween-20 in PBS (PBST) three times for 5 min each and then incubated in Tris/HCL (pH 9) over night. Slides were washed again with PBST and centrifuged to dry. Slides were blocked with 5% BSA in PBST for 1 h at 4°C. Silicon gaskets and bottomless 16-well plates (Grace Bio-Labs) were attached and microarrays incubated in primary antibodies. Each microarray was probed with a rabbit antibody against the target protein (See Table S2 for antibody list) and mouse anti-β-actin (Cell Signaling Technologies) at 1:1000 in 5% BSA in PBST for 24 hours at 4°C. The antibodies chosen were previously validated to minimize this cross-reactivity. Slides were washed three times with PBST and incubated with secondary antibodies AlexaFluor-647 donkey anti-rabbit and AlexaFluor-555 goat anti-mouse (ThermoFisher) at 1:1000 in 5% BSA in PBST for 24 h at 4°C. Slides were washed again and centrifuged dry. Slides were scanned using an Axon Genepix 400B Scanner. Spots were identified and intensities quantified using Innopsis Mapix software.

In vitro immunofluorescence and quantification

3×10^5 Hepa1-6 cells were seeded in each well of an 8-well Permanox chamber slide (NUNC Inc.). Cells were infected with 5×10^4 *P. yoelii* 17XNL sporozoites. Slides were centrifuged for 3 min at 515*g* in a hanging-bucket centrifuge to aid in sporozoite invasion. After 90 min, media containing extracellular sporozoites was aspirated, and fresh media containing drug or vehicle, was added. Media and drugs were changed every 24 h. LSs developed for 24 or 48 h, at which time cells were fixed with 10% formalin, blocked and permeabilized for 1 in PBS containing 0.1% Triton X-100 and 2% bovine serum albumin (BSA). Staining steps were performed in PBS supplemented with 2% BSA. Cells were stained using anti-sera to *Plasmodium* heat shock protein 70 (HSP70) at 4°C overnight, then visualized with the use of AlexaFluor-488 goat anti-mouse secondary antibody (Invitrogen). Cells were stained with DAPI to visualize both hepatocyte and parasite nuclei.

Flow cytometry of infected and uninfected cells

5×10^5 Hepa1-6 cells were seeded in each well of a 24-well plate (Corning). After infection and/or treatment cells were harvested with 0.25%Trypsin-EDTA and fixed with Cytoperm/Cytofix (BD Biosciences). The cells were blocked with Perm/Wash (BD Biosciences) +2% BSA for one h at room temperature then stained overnight at 4°C with primary antibodies. Cells were washed three times with PBS then stained for one hour at room temperature with secondary antibodies. The cells were washed and suspended in PBS+5 mM EDTA. For ploidy measurements, RNase A (0.1 mg/mL) and FxCycle Far Red Stain (Invitrogen) were added to the resuspension medium. Infection rate, protein signal, and DNA content were measured by flow cytometry on an LSRII (Becton-Dickson) and analyzed by FlowJo (Tree Star). Antibodies used include rabbit anti-p-RPS6 (S235/6) at 1:200 (Cell Signaling Technologies), mouse anti-RPS6 at 1:100, (Cell Signaling Technologies), mouse anti-β-actin (Cell Signaling Technologies), *T. gondii* P30 mouse monoclonal antibody at 1:1000 (Novus Biologicals), goat anti-mouse conjugated to AlexaFluor 488 (Invitrogen) at 1:1000, donkey anti-rabbit conjugated to AlexaFluor 647 (Invitrogen) at 1:1000, and a monoclonal antibody to *P. yoelii* Circumsporozoite protein (CSP) conjugated to AlexaFluor 488 (Life Technologies) at 1:500. Anti-β-actin and anti-p-RPS6 antibodies were not cross-reactive with extracellular *P. yoelii* sporozoites or *T. gondii* tachyzoites (Figure S6).

Immunofluorescence Microscopy

Extracellular sporozoites and tachyzoites were fixed and stained with antibodies as described above. Images were acquired with a 100 × 1.4 NA objective (Olympus) on a DeltaVision Elite High Resolution Microscope (GE Healthcare Life Sciences). The sides of each pixel represent 64.5 × 64.5 nm and z stacks were acquired at 300 nm intervals. Approximately 10 slices were acquired per image stack. For deconvolution, the 3D datasets were processed to remove noise and reassign blur by an iterative Classic Maximum Likelihood Estimation widefield algorithm provided by Huygens Professional Software (Scientific Volume Imaging BV, the Netherlands).

Western blotting

For BALB/c blots, whole liver lysate was gathered as described above. For drug treatments, $1x10^6$ Hepa1-6 cells were seeded in each well of a 6-well plate. Drugs or a DMSO control were added to the medium, and cells were incubated for 22 h. Insulin-transferrin-sodium selenite (ITSS) was then added to the medium for 30 min to stimulate cells. Media was aspirated and cells were lysed in an SDS lysis buffer at 4°C for 30 min, then at room temperature for 30 min. Lysate was harvested and filtered in AcroPrep Advance filter plates (Pall Corporation) spun for 45 min at 3500 rpm. 4x Western Loading Dye (Invitrogen) was added and lysates were boiled for 5 min. Proteins were run on Bolt 4%–12% Bis-Tris Plus gels (Invitrogen), then transferred using the iBlot dry transfer system (Invitrogen).

Membranes were briefly rinsed in methanol then blocked for 1 h at room temperature in TBS+0.5% Tween-20+5% BSA. Primary antibodies were added and incubated at 4°C overnight. All primary antibodies were obtained from Cell Signaling Technologies, and were used at a 1:1000 working concentration. Blots were then washed 3x 10 minutes in TBS-Tween, then incubated in TBS-Tween-BSA with secondary antibodies (anti-mouse 800, 1:10,000 and anti-rabbit 680, 1:10,000; Li-Cor). Blots were washed a second time, allowed to dry, and visualized and analyzed on an Odyssey IR scanner (Li-Cor). Protein levels were quantified by measuring IR signal and all data were normalized to β-actin. Antibodies for p-RPS6 and β-actin were incubated with and found to have no reactivity against extracellular *P. yoelii* sporozoites or *T. gondii* tachyzoites (Figure S6).

In vivo treatment and infection

Drugs were prepared by initial suspending in DMSO to a stock solution, then diluting the stock in warmed PBS and Tween-80, gently pipetting to avoid precipitation. Final vehicle was 2% DMSO+5% Tween-80+drug: BI-D1840 (50 mg/kg) or LY2584702 tosylate (12.5 mg/kg). Drug was injected intraperitoneally every 24 h at days −1, 0, and 1. At day 0, $5x10^4$ *P. yoelii* GFP-Luc sporozoites were injected via tail vein. Liver stage burden of *PyGFP-luc* development was monitored by *in vivo* bioluminescence imaging (IVIS) as described below.

In vivo bioluminescent imaging of liver-stage development

Luciferase activity in animals was visualized through imaging of whole bodies using the *in vivo* Imaging System (Caliper Life Sciences). Mice were injected intraperitoneally with 100 μL of RediJect D-Luciferin (Perkin Elmer) prior to being anesthetized using the isoflurane-anesthesia system (XGI-8, Caliper Life Sciences). Bioluminescence images were acquired with a 10 cm field of view, medium binning factor, and an exposure time of 3–5 min. Quantitative analysis of bioluminescence was performed by measuring the luminescence signal intensity using the region of interest (ROI) settings of the Living Image 3.0 software. ROIs were placed around the abdominal area at the location of the liver and background luminescence subtracted based on background ROI measurements on the lower abdomen.

QUANTIFICATION AND STATISTICAL ANALYSIS

Innopsis Mapix software was used to quantify lysate array spot signal intensity. Living Image 3.0 software was used to quantify luciferase activity in infected mice. An iterative Classic Maximum Likelihood Estimation widefield algorithm provided by Huygens Professional Software was used to process immunofluorescence images of sporozoites, as described in the immunofluorescence microscopy method details section. FlowJo was used to visualize and quantify all flow cytometry data. Representative FlowJo plots are shown in Figures S1 and S4. GraphPad Prism 7 was used for all statistical analyses. Statistical details for each experiment can be found in the figure legends, including the number of technical and biological replicates performed.

For *in vivo* experiments a biological replicate consisted of an individual mouse or, for LS size measurement, individual parasites. For *in vitro* experiments 3 or more biological replicates were performed, using separate passages of cells and parasites. For *in vitro* experiments three technical replicates (wells of cells plated, infected, and treated side by side) were performed in each biological replicate. For protein lysate arrays quadruplicate technical replicates of each biological replicate were printed and the mean signal used. Means and individual data points are shown on all bar graphs. Standard error is shown in Table 1. Data were analyzed using Student's t test, linear regression, or Pearson's Correlation Coefficient as indicated in the figure legends. No data points were excluded. P value < 0.05 was used as the statistical significance threshold.